

Supporting Information

Fe-Doping Induced Morphology Change, Oxygen Vacancy and Ce³⁺- Ce³⁺ Pairs in CeO₂ for Promoted Electrocatalytic Nitrogen Fixation

Ke Chu *, Yong-hua Cheng, Qing-qing Li, Ya-ping Liu, Ye Tian

*School of Materials Science and Engineering, Lanzhou Jiaotong University, Lanzhou 730070,
China*

*Corresponding author. E-mail address: chukelut@163.com (K. Chu)

Experimental section

Synthesis of Fe-CeO₂

All the chemicals were used as received without further purification. Briefly, 0.37 g of Ce(NO₃)₂·6H₂O and 18.6 mg of Fe(NO₃)₂·6H₂O were dissolved in 50 mL of deionized water under vigorously stirring for 5 min to form a transparent solution. The mixed solution was transferred into a Teflon-lined stainless-steel autoclave and kept at 180 °C for 24 h. After the autoclave was naturally cooled down to room temperature, the obtained samples were cleaned with deionized water several times and then calcined in a muffle furnace at 300 °C for 3 h under air atmosphere. For comparison, the pristine CeO₂ were fabricated by the same procedure without addition of Fe(NO₃)₂·6H₂O.

Electrochemical measurements

Electrochemical measurements were carried out on a CHI-660E electrochemical workstation with a standard three-electrode system, where catalyst coated on carbon cloth (CC) was used as working electrode, graphite rod as counter electrode and Ag/AgCl as reference electrode. The carbon cloth (CC, 1 × 1 cm²) was pretreated by soaking it in 0.5 M H₂SO₄ for 12 h, and then washed with deionized water several times and dried at 60 °C for 24 h. The catalyst ink was prepared by dispersing 1 mg of the catalyst in 100 μL of ethyl alcohol containing 5 μL of Nafion (5 wt%) under ultrasonication. The 20 μL of the catalyst ink was then deposited onto pretreated CC and dried in the air. All potentials were referenced to the reversible hydrogen electrode (RHE), which was performed in the high-purity hydrogen saturated 0.5 M LiClO₄ electrolyte by cyclic voltammeters curves, with using graphite rod and Pt wire as counter and working electrodes, respectively (Fig. S2). The NRR measurements were conducted in an H-type electrochemical cell separated by a Nafion 211 membrane (Fig. S1). An absorber was set at the end of cell to avoid the loss of produced NH₃ by N₂ flow. Prior to electrolysis, the cathodic compartment was purged with Ar for 30 min. During the electrolysis, ultra-high-purity N₂ gas (99.999%) was continuously purged into the cathodic chamber at a flow rate of 20 mL min⁻¹. After

NRR electrolysis, the solution in absorber was poured back into the cathodic compartment for the NH₃ detection.

Determination of NH₃

Typically, 4 mL of electrolyte was removed from the electrochemical reaction vessel. Then 50 μL of solution containing NaOH (0.75 M) and NaClO ($\rho_{\text{Cl}} = \sim 4.5$), 500 μL of solution containing 0.32 M NaOH, 0.4 M C₇H₆O₃Na, and 50 μL of C₅FeN₆Na₂O solution (1 wt%) were respectively added into the electrolyte. After standing for 2 h, the UV-Vis absorption spectrum was measured and the concentration-absorbance curves were calibrated by the standard NH₄Cl solution with a series of concentrations.

NH₃ yield was calculated by the following equation:

$$\text{NH}_3 \text{ yield } (\mu\text{g h}^{-1} \text{ mg}_{\text{cat}}^{-1}) = \frac{c_{\text{NH}_3} \times V}{t \times m} \quad (1)$$

Faradaic efficiency was calculated by the following equation:

$$\text{Faradaic efficiency } (\%) = \frac{3 \times F \times c_{\text{NH}_3} \times V}{17 \times Q} \times 100\% \quad (2)$$

where c_{NH_3} (μg mL⁻¹) is the measured NH₃ concentration, V (mL) is the volume of the electrolyte, t (h) is the reduction time and m (mg) is the mass loading of catalyst on carbon paper. F (96500 C mol⁻¹) is the Faraday constant, Q (C) is the quantity of applied electricity.

Determination of N₂H₄

Typically, 5 mL of electrolyte was removed from the electrochemical reaction vessel. The 330 mL of color reagent containing 300 mL of ethyl alcohol, 5.99 g of C₉H₁₁NO and 30 mL of HCl were prepared, and 5 mL of color reagent was added into the electrolyte. After stirring for 10 min, the UV-Vis absorption spectrum was measured and the concentration-absorbance curves were calibrated by the standard N₂H₄ solution with a series of concentrations.

Characterizations

Transmission electron microscopy (TEM), high-resolution transmission electron microscopy (HRTEM) and high-angle annular dark field-scanning transmission

electron microscopy (HAADF-STEM) were performed on a Tecnai G² F20 microscope. X-ray diffraction (XRD) pattern was recorded on a Rigaku D/max 2400 diffractometer. Nitrogen adsorption/desorption isotherms were recorded on an ASAP 2020 instrument. X-ray photoelectron spectroscopy (XPS) analysis was conducted on a PHI 5702 spectrometer. Photoluminescence spectra were recorded on a FLS-920T fluorescence spectrophotometer. Electron paramagnetic resonance (EPR) measurements were performed on a Bruker ESP-300 spectrometer. ¹H nuclear magnetic resonance (NMR) measurements were conducted on a 500 MHz Bruker superconducting-magnet NMR spectrometer. Prior to NMR measurement, ¹⁵N₂ gas (99% isotopic purity) was purified by an acid trap (0.05 M H₂SO₄) before entering the electrochemical chamber.

Calculation details

Spin-polarized density functional theory (DFT) calculations were performed on a Cambridge sequential total energy package (CASTEP)[1]. The generalized gradient approximation (GGA) within the framework of Perdew–Burke–Ernzerhof (PBE) functional was used for the description of exchange-correlation potential. The van der Waals (vdW) interaction was considered by a DFT-D method. The Brillouin zone was sampled with 3 × 3 × 1 k-points, and a kinetic cutoff energy was set as 500 eV. Electronic energies were computed with the tolerance of 2 × 10⁻⁵ eV and total force of 0.01 eV/Å. The effective Hubbard U_{eff} value of 5.0 eV ($U=5$ eV, $J=0$ eV) was applied for Ce4f states [2]. The eight-layered CeO₂ (111) with a 3×3 supercell is explored for slab modeling, in which the bottom five slabs are fixed while the top three slabs are allowed to relax. A vacuum space of 15 Å was adopted to avoid interactions between periodic images.

The computational hydrogen electrode (CHE) model was used to calculate the Gibbs free energy change (ΔG) of reaction steps:

$$\Delta G = \Delta E + \Delta ZPE - T\Delta S + \Delta G_{\text{U}} + \Delta G_{\text{pH}} \quad (3)$$

where ΔE is the electronic energy difference, ΔZPE is the zero point energy difference, T is the room temperature (298 K) and ΔS is the entropy change. ΔG_{U} is

the contribution of electrode potential, which can be calculated by: $\Delta G_U = -eU$, where U is the applied potential. ΔG_{pH} is the free energy correction of pH, which can be calculated by: $\Delta G_{\text{pH}} = -k_B T \times \text{pH} \times \ln 10$, where k_B is the Boltzmann constant, and the value of pH was set to be 7 for neutral medium used in our work. The transition state of water dissociation was analyzed by a combined linear synchronous transit (LST) and quadratic synchronous transit (QST) tools.

The formation energy (E_f) of $\text{CeO}_2\text{-V}_o$, $\text{Fe-CeO}_2\text{-V}_o$ and Fe-CeO_2 can be defined as:

$$E_f(\text{CeO}_2\text{-V}_o) = E(\text{CeO}_2\text{-V}_o) - E(\text{CeO}_2) + \mu_{\text{O}} \quad (4)$$

$$E_f(\text{Fe-CeO}_2\text{-V}_o) = E(\text{Fe-CeO}_2\text{-V}_o) - E(\text{CeO}_2) - \mu_{\text{Fe}} + \mu_{\text{Ce}} + \mu_{\text{O}} \quad (5)$$

$$E_f(\text{Fe-CeO}_2) = E(\text{Fe-CeO}_2) - E(\text{CeO}_2) - \mu_{\text{Fe}} + \mu_{\text{Ce}} \quad (6)$$

where E is the total energies of corresponding structures, μ is the chemical potential of corresponding atoms.

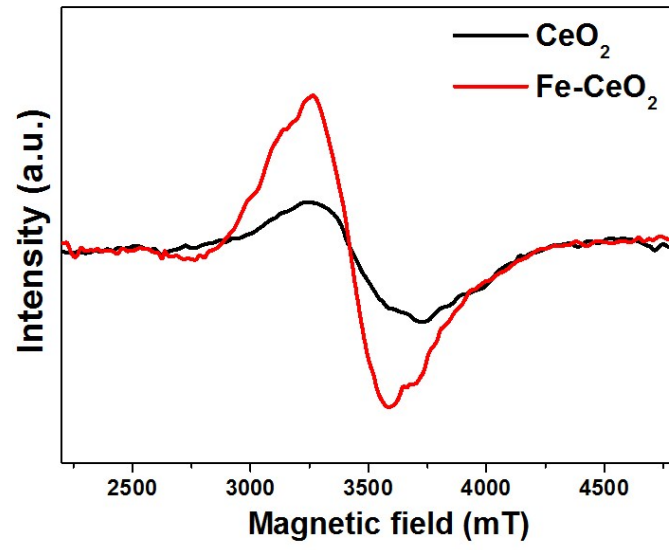


Fig. S1. EPR spectra of CeO_2 and Fe-CeO_2 .

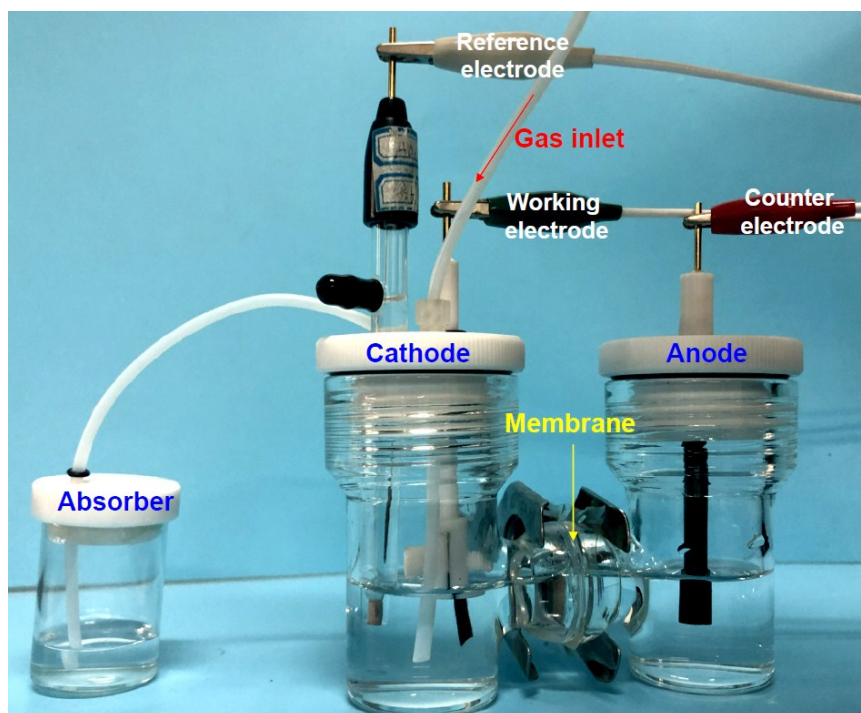


Fig. S2. Photograph of H-type electrochemical setup.

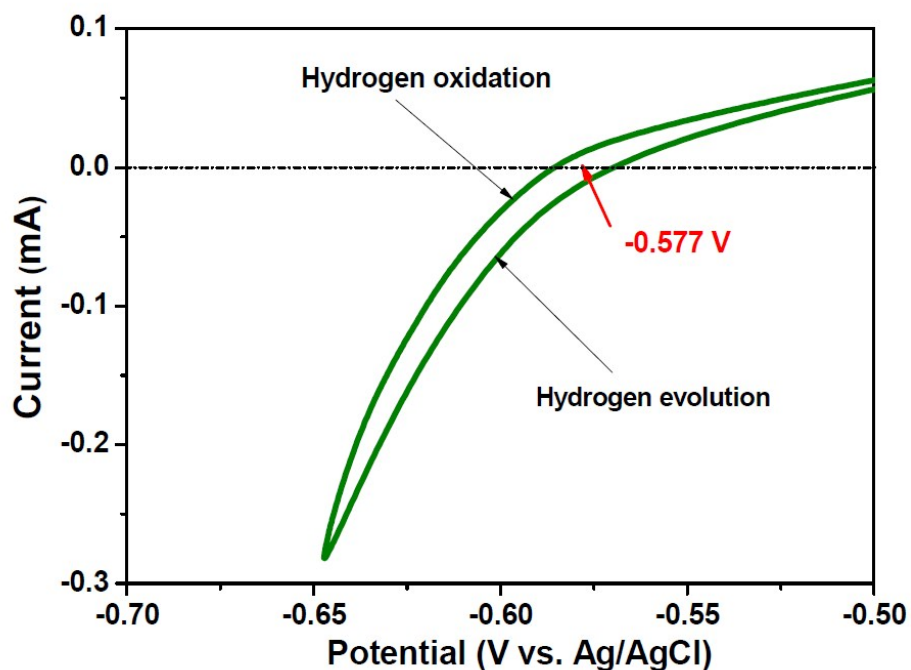


Fig. S3. The RHE calibration in 0.5 M LiClO₄ electrolyte.

The RHE calibration was conducted in the high-purity hydrogen saturated 0.5 M LiClO₄ electrolyte. The graphite rod and Pt wire were used as the counter and working electrodes, respectively. The cyclic voltammetry curves were performed at a scan rate of 1 mV s⁻¹. The RHE calibration potential for the hydrogen oxidation/evolution reactions is the average value of the two potentials at which the current crosses zero. It is shown in Fig. S2 that the $E(\text{RHE})$ is larger than $E(\text{Ag/AgCl})$ by 0.577 V. Therefore, we have

$$E(\text{RHE}) = E(\text{Ag/AgCl}) + 0.577.$$

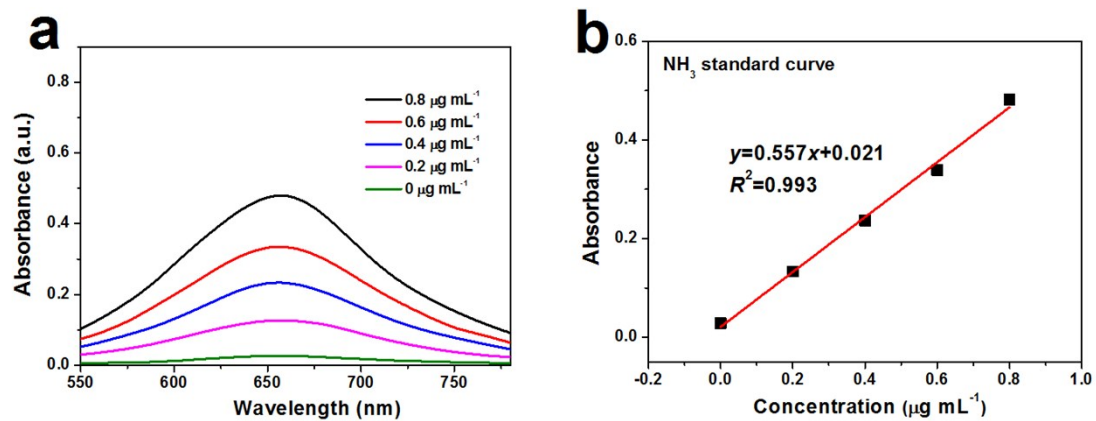


Fig. S4. (a) UV-Vis absorption spectra of indophenol assays with NH_4Cl after incubated for 2 h at ambient conditions. (b) Calibration curve used for calculation of NH_3 concentrations.

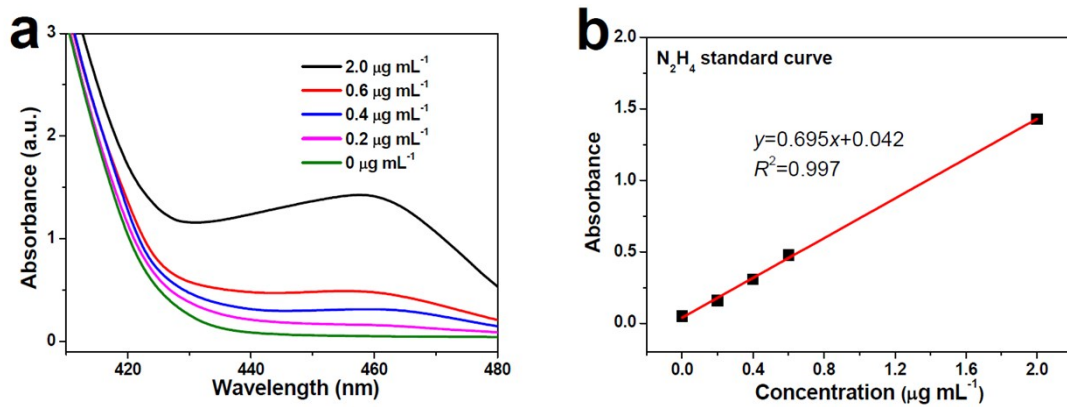


Fig. S5. (a) UV-Vis absorption spectra of N_2H_4 assays after incubated for 20 min at ambient conditions. (b) Calibration curve used for calculation of N_2H_4 concentrations.

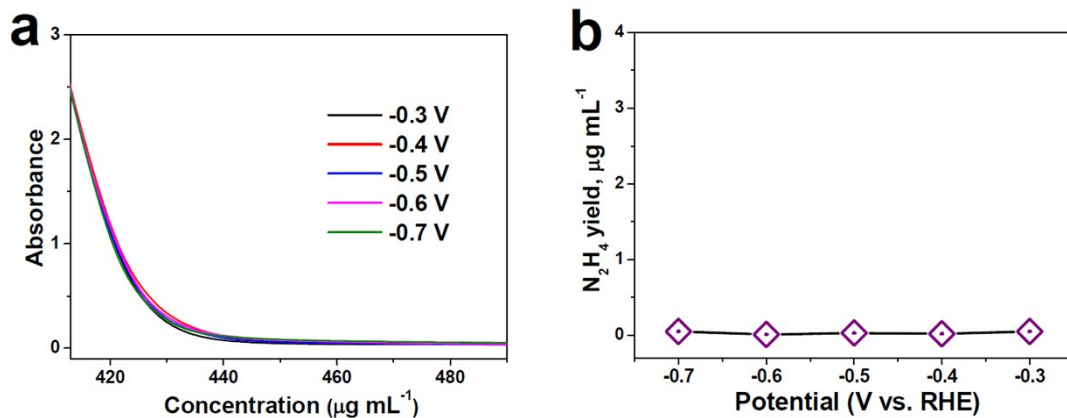


Fig. S6. (a) UV-Vis spectra of the electrolytes (stained with the chemical indicator based on the method of Watt and Chrisp) after 2 h electrocatalysis on Fe-CeO₂ at various potentials, and (b) corresponding N₂H₄ concentrations in the electrolytes.

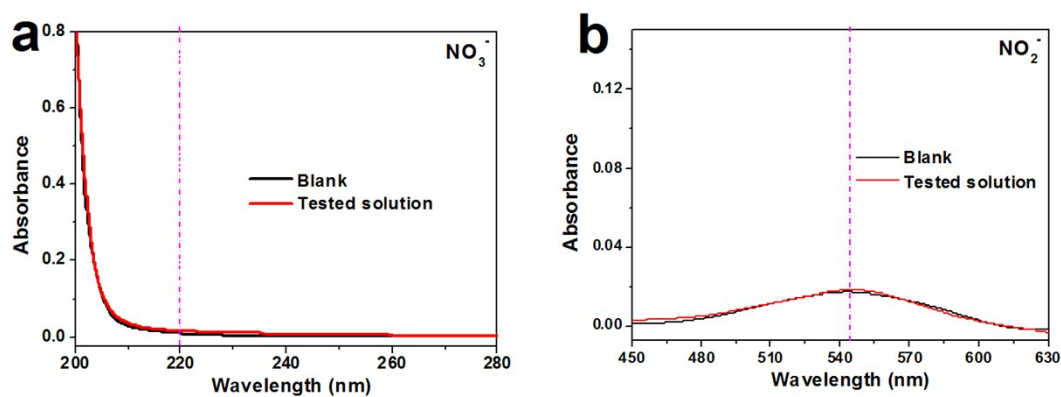


Fig. S7. UV-vis absorption spectra for the determination of (a) NO_3^- and (b) NO_2^- in blank (deionized water) and tested solution.

The concentration of the NO_3^- and NO_2^- could be quantitatively determined by the well-established spectrophotometer measurement[3]. For determining NO_3^- , 5.0 mL of standard LiNO_3 solution was added into 0.10 mL of 1.0 M HCl. After standing for 5 min, the concentration of NO_3^- was measured by UV-vis spectrophotometer at wavelength range from 200 to 280 nm. For determining NO_2^- , 5.0 mL of standard LiNO_2 was added into 0.10 mL of sulfanilamide solution containing (0.50 g of sulfanilamide dissolved in 50.0 mL of 2.0 M HCl), followed by the addition of N-(1-naphthyl) ethylenediamine dihydrochloride solution (20.0 mg of N-(1-Naphthyl) ethylenediamine dihydrochloride dissolved in 20.0 mL of deionized water). After standing for 30 min, the concentration of NO_2^- was measured by UV-vis spectrophotometer at wavelength range from 450 to 630 nm.

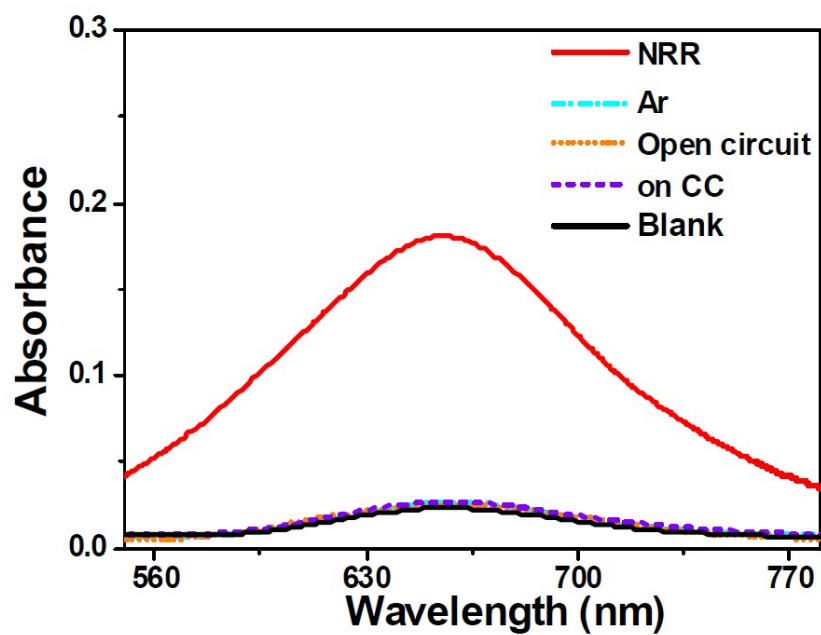


Fig. S8. UV-Vis absorption spectra of working electrolytes after 2 h of electrolysis on Fe-CeO₂ at -0.5 V in N₂-saturated solution, Ar-saturated solutions, N₂-saturated solution at open circuit, N₂-saturated solution on pristine CC and blank data.

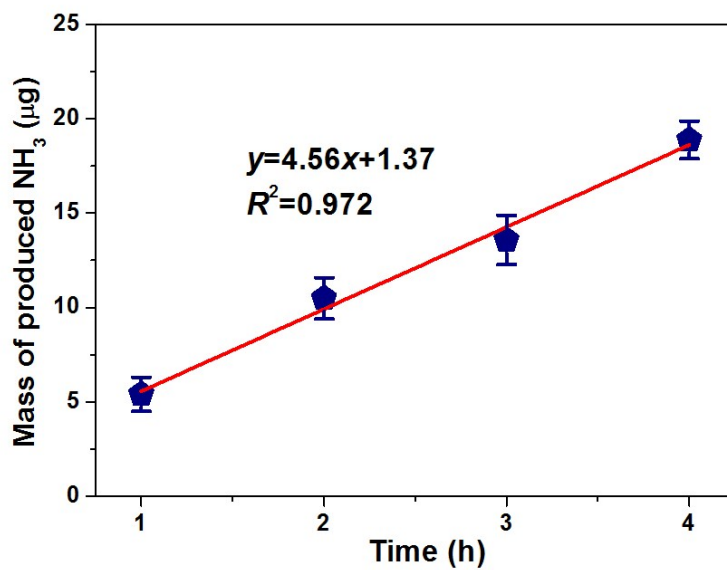


Fig. S9. The mass of produced NH₃ after electrolysis at various times on Fe-CeO₂ at -0.5 V. The error bars correspond to three separately measurements under the identical conditions.

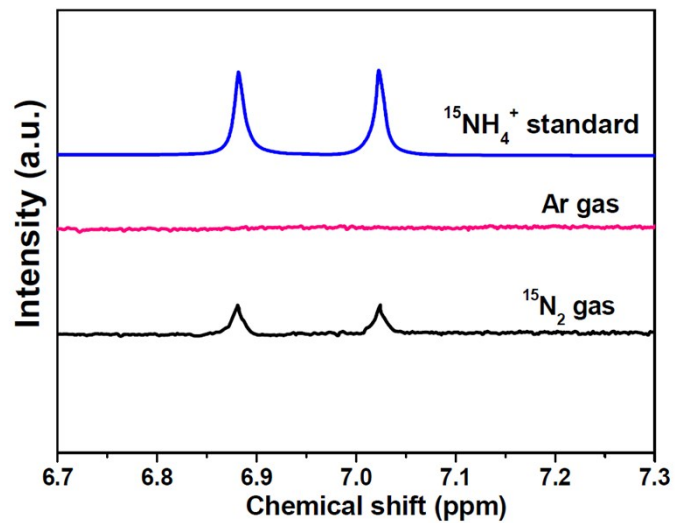


Fig. S10. ^{15}N NMR spectra of $^{15}\text{NH}_4^+$ standard samples, and the electrolytes after 2 h of NRR electrolysis on Fe-CeO₂ using Ar and $^{15}\text{N}_2$ as feeding gases.

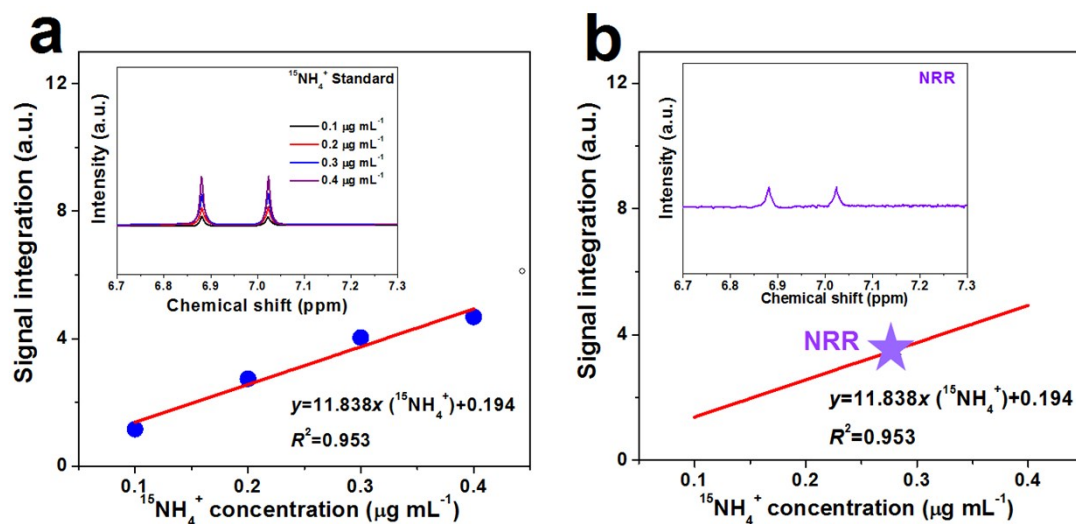


Fig. S11. (a) ^1H NMR spectra of $^{15}\text{NH}_4^+$ standard samples with different concentrations (inset), and corresponding calibration curve of $^{15}\text{NH}_4^+$ concentration vs. peak area. (b) ^1H NMR spectra of the electrolyte after NRR electrolysis on Fe-CeO₂ for 2 h at -0.5 V (inset), and the determined $^{15}\text{NH}_4^+$ concentrations of the electrolyte by referring to the calibration curve. The NMR determined value is 0.262 $\mu\text{g mL}^{-1}$, agreeing well with 0.279 $\mu\text{g mL}^{-1}$ determined by the indophenol blue method within the reasonable margin of experimental error.

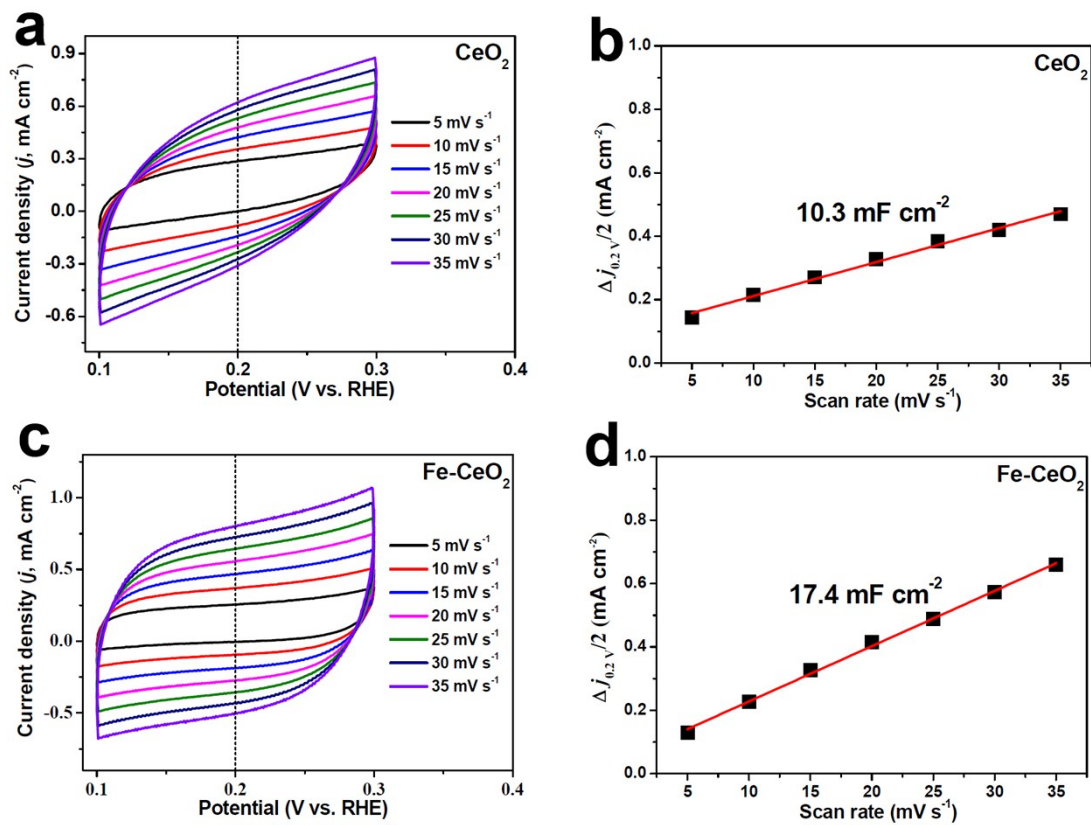


Fig. S12. Electrochemical double-layer capacitance (C_{dl}) measurements with different scanning rates of 5~35 mV s⁻¹ for (a, b) CeO₂ and (c, d) Fe-CeO₂.

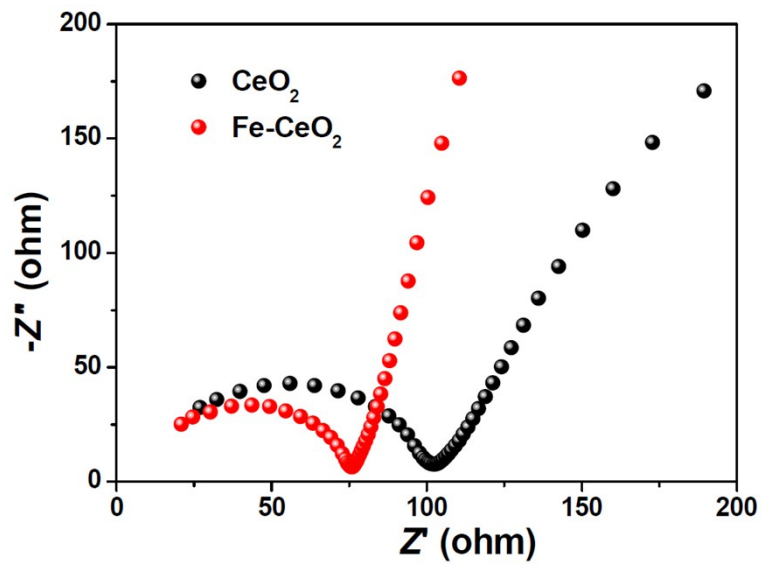


Fig. S13. Electrochemical impedance spectra of CeO_2 and Fe-CeO_2 .

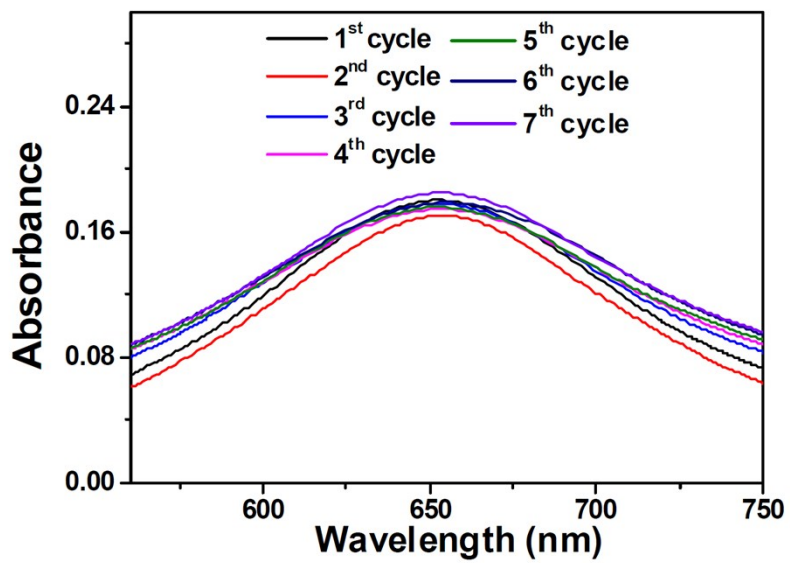


Fig. S14. UV-Vis absorption spectra of working electrolytes on Fe-CeO₂ (each for 2 h electrolysis at -0.5 V) for seven cycles.

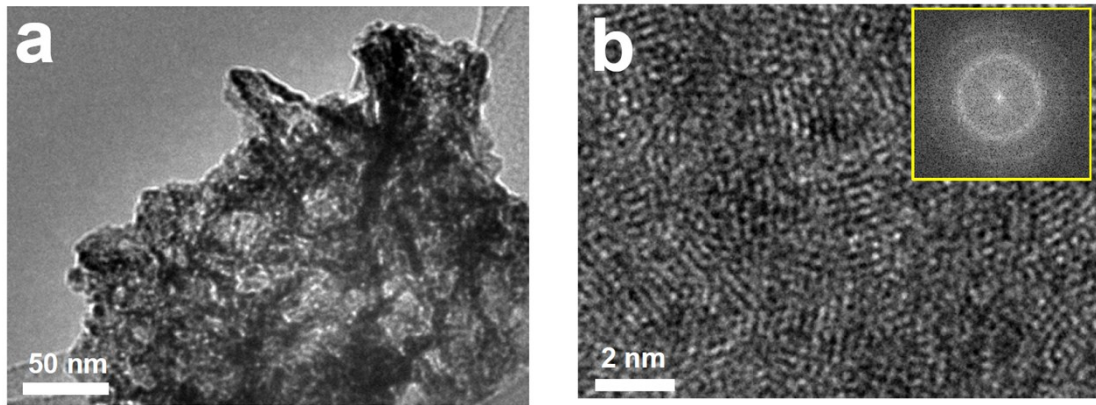


Fig. S15. Morphology of Fe-CeO₂ after stability test. (a) TEM image. (b) HRTEM image (inset: FFT)

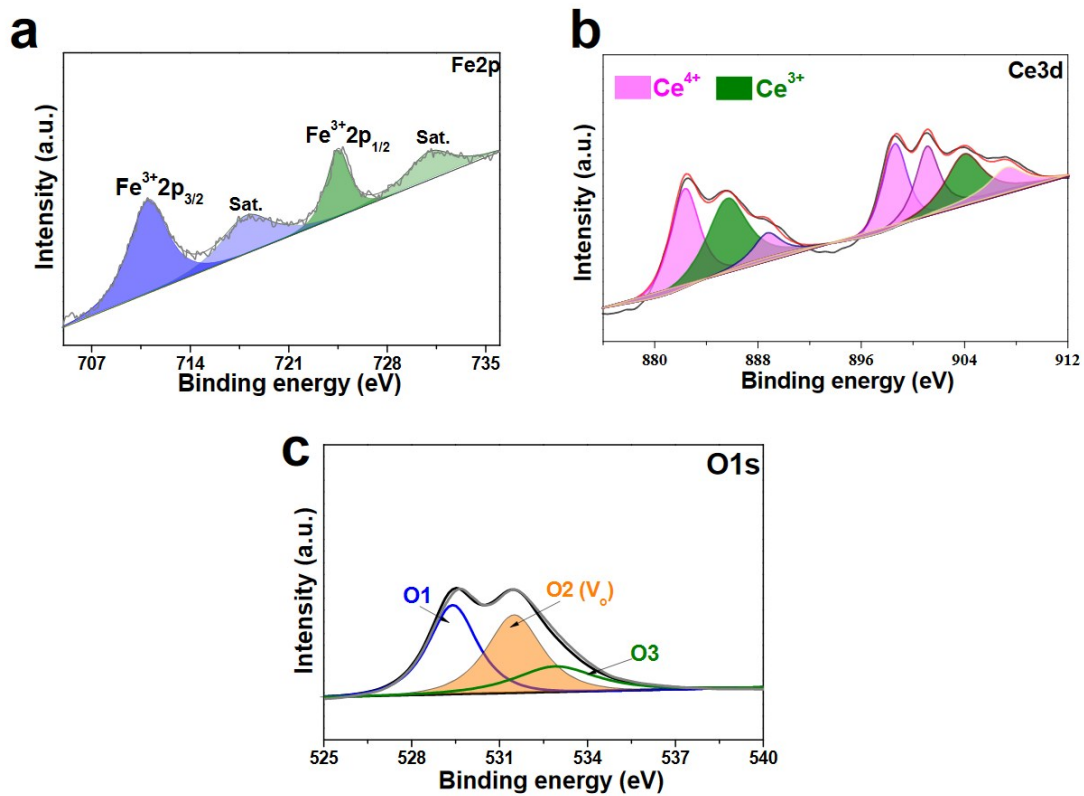


Fig. S16. XPS spectra of Fe-CeO₂ after stability test: (a) Fe2p; (b) Ce3d; (c) O1s.

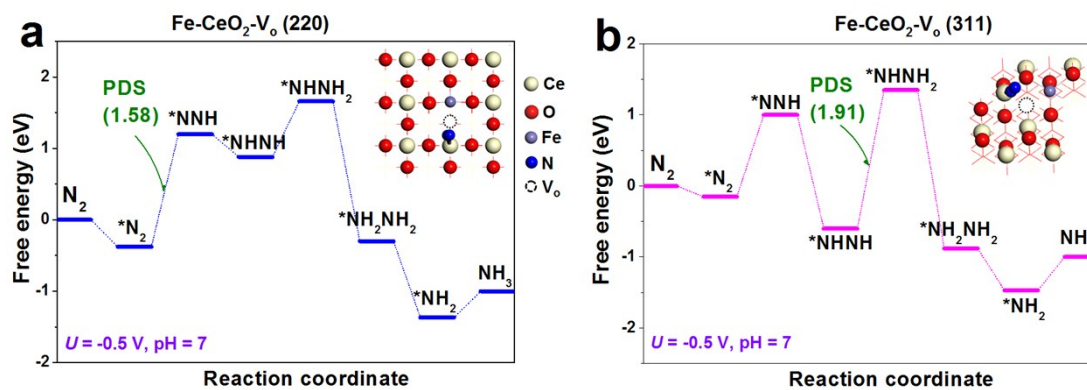


Fig. S17. Free energy diagrams of NRR pathways on (220) and (311) planes of energetically stable Fe-CeO₂-V_o and their corresponding N₂ adsorption configurations (insets). (a) (220) plane; (b) (311) plane.

Table S1. Comparison of NH₃ yield and Faradic efficiency (FE) for recently reported metal-based NRR electrocatalysts at ambient conditions

Catalyst	Electrolyte	Determination method	Optimum Potential (V vs RHE)	NH ₃ yield	FE (%)	Ref.
Pd/C	0.1 M PBS	Indophenol blue method	0.1	4.5 μg h ⁻¹ mg ⁻¹	8.2	[4]
CoP hollow nanocage	1.0 M KOH	Indophenol blue method	-0.4	10.78 μg h ⁻¹ mg ⁻¹	7.36	[5]
Fe-N/C hybrid	0.1 M KOH	Indophenol blue method	-0.2	34.83 μg h ⁻¹ mg ⁻¹	9.28	[6]
Sulfur dots-graphene nanohybrid	0.5 M LiClO ₄	Indophenol blue method	-0.85	28.56 μg h ⁻¹ mg ⁻¹	7.07	[7]
Cr ₂ O ₃ /RGO	0.1 M HCl	Indophenol blue method	-0.6	33.3 μg h ⁻¹ mg ⁻¹	7.33	[8]
MoO ₂ with oxygen vacancies	0.1 M HCl	Indophenol blue method	-0.15	12.2 μg h ⁻¹ mg ⁻¹	8.2	[9]
Mosaic Bi nanosheets	0.1 M Na ₂ SO ₄	Indophenol blue method	-0.8	13.23 μg h ⁻¹ mg ⁻¹	10.46	[10]
Ru single atoms/NPC	0.05 M H ₂ SO ₄	Indophenol blue method	-0.2	120.9 μg h ⁻¹ mg ⁻¹	29.6	[11]
MoO ₃ nanosheets	0.1 M HCl	Indophenol blue method	-0.5	29.43 μg h ⁻¹ mg ⁻¹	1.9	[12]
Mo ₂ C/C	0.5 M Li ₂ SO ₄	Nessler's reagent method	-0.3	11.3 μg h ⁻¹ mg ⁻¹	7.8	[13]
Black phosphorus	0.01 M HCl	Indophenol blue method	-0.7	31.37 μg h ⁻¹ mg ⁻¹	5.07 (-0.6 V)	[14]
Mo ₂ N nanorods	0.1 M HCl	Indophenol blue method	-0.3	78.4 μg h ⁻¹ mg ⁻¹	4.5	[15]
B ₄ C nanosheet	0.1 M HCl	Indophenol blue method	-0.75	26.57 μg h ⁻¹ mg ⁻¹	15.95	[16]
TiO ₂ -rGO	0.1 M Na ₂ SO ₄	Indophenol blue method	-0.9	15.13 μg h ⁻¹ mg ⁻¹	3.3	[17]
Mosaic Bi nanosheets	0.1 M Na ₂ SO ₄	Indophenol blue method	-0.8	13.23 μg h ⁻¹ mg ⁻¹	10.46	[10]
Defective rich C ₃ N ₄	0.1 M HCl	Indophenol blue method	-0.2	8.09 μg h ⁻¹ mg ⁻¹	11.59	[18]
Mesoporous boron nitride	0.1 M Na ₂ SO ₄	Indophenol blue method	-0.7	18.2 μg h ⁻¹ mg ⁻¹	5.5	[19]
Mesoporous boron	0.1 M	Indophenol blue	-0.7	18.2	5.5	[19]

nitride	Na ₂ SO ₄	method		μg h ⁻¹ mg ⁻¹		
Boron nitride nanosheet	0.1 M HCl	Indophenol blue method	-0.75	22.4 μg h ⁻¹ mg ⁻¹	4.7	[20]
Bi ₄ V ₂ O ₁₁ -CeO ₂ nanofibers	0.1 M HCl	Indophenol blue method	-0.2	23.21 μg h ⁻¹ mg ⁻¹	10.16	[21]
Au/CeO _x -RGO	0.1 M KOH	Salicylate method	-0.2	8.31 μg h ⁻¹ mg ⁻¹	10.1	[22]
Au@CeO ₂	0.01 M H ₂ SO ₄	Indophenol blue method	-0.4	28.2 μg h ⁻¹ mg ⁻¹	9.5	[23]
Cu-doped CeO ₂	0.1 M Na ₂ SO ₄	Indophenol blue method	-0.45	13.3 μg h ⁻¹ mg ⁻¹	19.1	[24]
CeO ₂ nanorod	0.1 M Na ₂ SO ₄	Indophenol blue method	-0.5	16.4 μg h ⁻¹ mg ⁻¹	3.7 (-0.4 V)	[25]
CeO ₂ /graphene	0.1 M Na ₂ SO ₄	Indophenol blue method	-0.7	16.98 μg h ⁻¹ mg ⁻¹	4.78	[26]
Cr-doped CeO ₂	0.1 M Na ₂ SO ₄	Indophenol blue method	-0.7	16.82 μg h ⁻¹ mg ⁻¹	3.84	[2]
Fe-doped CeO₂	0.5 M Li₂SO₄	Indophenol blue method	-0.5	26.2 μg h⁻¹ mg⁻¹ 4.54 μg cm⁻² h⁻¹	14.7 (-0.4 V)	This work

Table S2. Calculated thermodynamic values for predicting the Gibbs free energies of various NRR intermediates over (111) plane of CeO₂-V_o (on Ce³⁺) according to Eq. (3).

	ΔE (eV)	ΔZPE (eV)	$T\Delta S$ (eV)	ΔG_U (eV)	ΔG_{pH} (eV)
*N ₂	-0.95	0.23	0.11	0.5	-0.42
*NNH	0.44	0.49	0.13	0.5	-0.42
*NHNH	0.14	0.88	0.12	0.5	-0.42
*NHNH ₂	-2.42	1.18	0.11	0.5	-0.42
*NH ₂ NH ₂	-2.06	1.55	0.12	0.5	-0.42
*NH ₂	-2.69	0.76	0.05	0.5	-0.42

Table S3. Calculated thermodynamic values for predicting the Gibbs free energies of various NRR intermediates over (111) plane of Fe-CeO₂-V_o (on Ce³⁺-Ce³⁺) according to Eq. (3).

	ΔE (eV)	ΔZPE (eV)	$T\Delta S$ (eV)	ΔG_U (eV)	ΔG_{pH} (eV)
*N-*N	-0.76	0.22	0.09	0.5	-0.42
*N-*NH	-0.25	0.46	0.13	0.5	-0.42
*NH-*NH	-0.06	0.85	0.12	0.5	-0.42
*NH-*NH ₂	-0.75	1.18	1.08	0.5	-0.42
*NH ₂ -*NH ₂	-1.12	1.45	0.15	0.5	-0.42
*NH ₂	-2.37	0.76	0.05	0.5	-0.42

Table S4. Calculated thermodynamic values for predicting the Gibbs free energies of various NRR intermediates over (111) plane of Fe-CeO₂-V_o (on Fe³⁺) according to Eq. (3).

	ΔE (eV)	ΔZPE (eV)	$T\Delta S$ (eV)	ΔG_U (eV)	ΔG_{pH} (eV)
*N ₂	-0.65	0.23	0.11	0.5	-0.42
*NNH	0.03	0.49	0.13	0.5	-0.42
*NHNH	-0.52	0.88	0.12	0.5	-0.42
*NHNH ₂	-0.94	1.18	0.11	0.5	-0.42
*NH ₂ NH ₂	-3.06	1.55	0.12	0.5	-0.42
*NH ₂	-3.11	0.76	0.05	0.5	-0.42

Table S5. Calculated thermodynamic values for predicting the Gibbs free energies of various NRR intermediates over (220) plane of Fe-CeO₂-V_o (on Ce³) according to Eq. (3).

	ΔE (eV)	ΔZPE (eV)	$T\Delta S$ (eV)	ΔG_U (eV)	ΔG_{pH} (eV)
*N ₂	-0.58	0.23	0.11	0.5	-0.42
*NNH	0.76	0.49	0.13	0.5	-0.42
*NHNH	0.04	0.88	0.12	0.5	-0.42
*NHNH ₂	0.51	1.18	0.11	0.5	-0.42
*NH ₂ NH ₂	-1.81	1.55	0.12	0.5	-0.42
*NH ₂	-2.16	0.76	0.05	0.5	-0.42

Table S6. Calculated thermodynamic values for predicting the Gibbs free energies of various NRR intermediates over (311) plane of Fe-CeO₂-V_o (on Ce³) according to Eq. (3).

	ΔE (eV)	ΔZPE (eV)	$T\Delta S$ (eV)	ΔG_U (eV)	ΔG_{pH} (eV)
*N ₂	-0.35	0.23	0.11	0.5	-0.42
*NNH	0.56	0.49	0.13	0.5	-0.42
*NHNH	-1.44	0.88	0.12	0.5	-0.42
*NHNH ₂	0.21	1.18	0.11	0.5	-0.42
*NH ₂ NH ₂	-2.39	1.55	0.12	0.5	-0.42
*NH ₂	-2.27	0.76	0.05	0.5	-0.42

Table S7. Calculated thermodynamic values for predicting the Gibbs free energies of various HER intermediates over Fe-CeO₂-V_o (on Ce³⁺-Ce³⁺) according to Eq. (3).

	Dissociation ΔE (eV)	ΔZPE (eV)	$T\Delta S$ (eV)	ΔG_U (eV)	ΔG_{pH} (eV)
H ₂ O dissociation	1.31	0.56	0.67	0.5	-0.42
*H	0.4	0.48	0.24	0.5	-0.42

Supplementary references

- [1]. S. J. Clark, M. D. Segall, C. J. Pickard, P. J. Hasnip, M. I. J. Probert, K. Refson and M. C. Payne, *Z. Kristallogr.*, 2005, **220**, 567-570.
- [2]. H. Xie, H. Wang, Q. Geng, Z. Xing, W. Wang, J. Chen, L. Ji, L. Chang, Z. Wang and J. Mao, *Inorg. Chem.*, 2019, **58**, 5423-5427.
- [3]. A. Carvalho, L. Meireles and F. X. Malcata, *Analisis*, 1998, **26**, 347-351.
- [4]. J. Wang, L. Yu, L. Hu, G. Chen, H. Xin and X. Feng, *Nat. Commun.*, 2018, **9**, 1795.
- [5]. W. Guo, Z. Liang, J. Zhao, B. Zhu, K. Cai, R. Zou and Q. Xu, *Small Methods*, 2018, **2**, 1800204.
- [6]. Y. Wang, X. Cui, J. Zhao, G. Jia, L. Gu, Q. Zhang, L. Meng, Z. Shi, L. Zheng and C. Wang, *ACS Catal.*, 2018, **9**, 336-344.
- [7]. H. Chen, X. Zhu, H. Huang, H. Wang, T. Wang, R. Zhao, H. Zheng, A. M. Asiri, Y. Luo and X. Sun, *Chem. Commun.*, 2019, **55**, 3152-3155.
- [8]. L. Xia, B. Li, Y. Zhang, R. Zhang, L. Ji, H. Chen, G. Cui, H. Zheng, X. Sun, F. Xie and Q. Liu, *Inorg. Chem.*, 2019, **58**, 2257-2260.
- [9]. G. Zhang, Q. Ji, K. Zhang, Y. Chen, Z. Li, H. Liu, J. Li and J. Qu, *Nano Energy*, 2019, **59**, 10-16.
- [10]. L. Li, C. Tang, B. Xia, H. Jin, Y. Zheng and S.-Z. Qiao, *ACS Catal.*, 2019, **9**, 2902-2908.
- [11]. Z. Geng, Y. Liu, X. Kong, P. Li, K. Li, Z. Liu, J. Du, M. Shu, R. Si and J. Zeng, *Adv. Mater.*, 2018, **30**, 1803498.
- [12]. J. Han, X. Ji, X. Ren, G. Cui, L. Li, F. Xie, H. Wang, B. Li and X. Sun, *J. Mater. Chem. A*, 2018, **6**, 12974-12977.
- [13]. H. Cheng, L. X. Ding, G. F. Chen, L. Zhang, J. Xue and H. Wang, *Adv. Mater.*, 2018, **30**, 1803694.
- [14]. L. L. Zhang, L. X. Ding, G. F. Chen, X. F. Yang and H. H. Wang, *Angew. Chem. Int. Edit.*, 2019, **131**, 2638-2642.
- [15]. X. Ren, G. Cui, L. Chen, F. Xie, Q. Wei, Z. Tian and X. Sun, *Chem. Commun.*, 2018, **54**, 8474-8477.
- [16]. W. Qiu, X.-Y. Xie, J. Qiu, W.-H. Fang, R. Liang, X. Ren, X. Ji, G. Cui, A. M. Asiri and G. Cui, *Nat. Commun.*, 2018, **9**, 3485.
- [17]. X. Zhang, Q. Liu, X. Shi, A. M. Asiri, Y. Luo, X. Sun and T. Li, *J. Mater. Chem. A*, 2018, **6**, 17303-17306.
- [18]. C. Lv, Y. Qian, C. Yan, Y. Ding, Y. Liu, G. Chen and G. Yu, *Angew. Chem. Int. Edit.*, 2018, **57**, 10246-10250.
- [19]. J. Zhao, X. Ren, X. Li, D. Fan, X. Sun, H. Ma, Q. Wei and D. Wu, *Nanoscale*, 2019, **11**, 4231-4235.
- [20]. Y. Zhang, H. Du, Y. Ma, L. Ji, H. Guo, Z. Tian, H. Chen, H. Huang, G. Cui, A. M. Asiri, F. Qu, L. Chen and X. Sun, *Nano Res.*, 2019, **12**, 919-924.
- [21]. C. Lv, C. Yan, G. Chen, Y. Ding, J. Sun, Y. Zhou and G. Yu, *Angew. Chem. Int. Edit.*, 2018, **130**, 6181-6184.
- [22]. S. J. Li, D. Bao, M. M. Shi, B. R. Wulan, J. M. Yan and Q. Jiang, *Adv. Mater.*, 2017, **29**, 1700001.
- [23]. G. Liu, Z. Cui, M. Han, S. Zhang, C. Zhao, C. Chen, G. Wang and H. Zhang, *Chem. Eur. J*, 2019, **25**, 5904-5911.

- [24]. S. Zhang, C. Zhao, Y. Liu, W. Li, J. Wang, G. Wang, Y. Zhang, H. Zhang and H. Zhao, *Chem. Commun.*, 2019, **55**, 2952-2955.
- [25]. B. Xu, L. Xia, F. Zhou, R. Zhao, H. Chen, T. Wang, Q. Zhou, Q. Liu, G. Cui, X. Xiong, F. Gong and X. Sun, *ACS Sustain. Chem. Eng.*, 2019, **7**, 2889-2893.
- [26]. H. Xie, Q. Geng, X. Li, T. Wang, Y. Luo, A. A. Alshehri, K. A. Alzahrani, B. Li, Z. Wang and J. Mao, *Chem. Commun.*, 2019, **55**, 10717-10720.